Nanolayers in Fiber-Optic Biosensing

Małgorzata Ję drzejewska-Szczerska[1], Daria Majchrowicz[1], Marzena Hirsch[1], Przemysław Struk[2], Robert Bogdanowicz[1], Mikhael Bechelany[3] and Valery V. Tuchin[4,5,6]

[1]*Gdańsk University of Technology, Gdańsk, Poland* [2]*Silesian University of Technology, Gliwice, Poland* [3]*Université de Montpellier, Montpellier, France* [4]*Saratov State University, Saratov, Russia* [5]*Institute of Precision Mechanics and Control RAS, Saratov, Russia* [6]*Tomsk State University, Tomsk, Russia*

Chapter Outline

14.1 Introduction

Optoelectronic methods, including classical spectroscopic techniques (absorption, fluorescence, and Raman spectroscopies) are widely used in medicine, especially for laboratory diagnostic tests and imaging. These measurements are costly—require expensive and special equipment and also additional elements necessary to take the analysis (e.g., reagents, dedicated trays, method of preparing samples of biological materials). Moreover, their proper use is possible only by the qualified personnel. There is a need to construct relatively cheap and easy-to-use measuring devices that may have worse parameters than metrological laboratory equipment but, due to the low price, would become more popular.

The use of fiber-optic sensors, as low-cost measuring devices in biology and medicine, is still insufficient and very desirable.

Fiber-optic sensors have several advantages in comparison to electronic sensors of the same size. Due to the fact that dielectric materials are used, they are insensitive to the electric and magnetic field that is generated by the devices used for medical diagnostics and therapy. Additionally, they are not sensitive in some limits to chemical agents and ionizing radiation. It is worth noting that the fiber-optic sensors can be implemented into transmitters of various physical quantities and they can usually be produced in a relatively cheap way. The small dimensions of such sensors (below hundreds of micrometers) allow one to avoid the appearance of distortions in the investigated area, allowing at the same realization of almost pointwise measurements. Furthermore, while using the spectrum analysis of the measured signal, such a sensor is insensitive to changes in the intensity of the optical signal in the transmission system, since all the information about the measured values is included in the frequency components of the measuring signal spectrum. Fiber-optic biosensors have significant advantages, as compared to the currently used electronic sensors:

- short measurement time which gives the opportunity to observe the dynamics of changes in the tissue parameters, e.g., dynamics of changes in blood flow or skin perspiration (Bosch et al., 2007);
- a lower required amount of the test substance (e.g., blood at the level of fractions of microliters instead of milliliters) (Tubchareon et al., 2013; Zanishevskaya et al., 2015);
- the ability to perform pointwise measurements;
- the lack of necessity for additional preparation of biological samples prior to the measurement, as a label-free DNA sensor (Wang et al., 2009);
- the ability to identify biological objects, such as bacteria, molecules, viruses, or antibodies, with very high sensitivity (Long et al., 2013; Shabaneh et al., 2015; Zheng et al., 2016);
- the potential noninvasive clinical applications in point-of-care testing, including the detection of bile-containing refluxes, gastric carbon dioxide, and interstitial pH (Baldini et al., 2008);
- immunity to external interferences (electromagnetic, mechanical stress, etc.) which makes it possible to use the sensor during medical diagnostics such as MRI (Avino et al., 2013).

On the other hand, in the last decade, fiber-optic sensors have gained popularity as biosensing devices. This has been made possible because of the integration of fiber-optic technology (such as photonic crystal fiber (Skibina et al., 2011) or long-period fiber grating (Janczuk-Richter et al., 2017)) and new materials. Those new materials, such as nanolayers and thin films, have been widely used in fiber-optic sensor technology where they can

play a role of a reflective, protective, or sensing layer. The metrological parameters of the fiber-optic interferometer (spatial resolution, accuracy) are determined mainly by the visibility of the measured signal. On the other hand, the visibility of measurement signal depends on the quality of the reflecting surface, especially of their refractive index as follows (Hariharan, 2003):

$$V = \frac{I_{max} - I_{min}}{I_{max} + I_{min}}, \tag{14.1}$$

$$I(\phi) = \frac{R_1 + R_2 - 2(R_1 R_2)^{1/2}\cos\phi}{1 + R_1 R_2 - 2(R_1 R_2)^{1/2}\cos\phi}, \tag{14.2}$$

$$I_{max}: \Delta\phi = 2m\pi, \tag{14.3}$$

$$I_{min}: \Delta\phi = (2m + 1)\pi, \tag{14.4}$$

$$R_1 = \left(\frac{n_2 - n_1}{n_1 + n_2}\right)^2, \tag{14.5}$$

$$R_2 = \left(\frac{n_3 - n_2}{n_2 + n_3}\right)^2, \tag{14.6}$$

where: I_{max}, I_{min}—maximum and minimum of the measured signal, respectively;

R_1, R_2—reflectance of the first and the second reflecting surfaces;
ϕ—phase difference between interfering light beams;
$n_{1,2,3}$—refractive indices of the fiber-optic core, medium, and thin film, respectively;
m—integer.

That is why mirrors and reflecting coatings which can act as a mirror are such important elements of the fiber-optic interferometers.

Usually a reflecting surface is made from silver. This material has limited resistance to chemicals and is sensitive to mechanical damage. Therefore, when the interferometer must be used in biosensing solution, the mirror must be biocompatible and possess chemical resistance. That is why the new materials for mirrors are strongly desired.

Secondly, thin films are used as protective coatings. Constructions of fiber-optic sensors, presented in literature, are dedicated most of all to industrial applications (Bohnert et al., 2005; Davanlou, 2014; Grattan, 2000) and cannot be used for investigating biological objects. In case of producing sensors for measuring parameters of biological objects, it is necessary to ensure the biocompatibility of the measuring head. This requires materials that do not cause inflammation, acute or chronic response of biological tissues, and are also nontoxic and resistant to the environment of tissues and body fluids. As materials with such

properties are mostly not available, then other materials have to be in the sensor's construction, the protective coating can be a solution. Finally, maybe the most common use of nanolayers and thin film for biosensing is their application as a sensing medium. In such a construction, any change in value of the measured quantity causes a change in the refractive index of the nanolayer, what can be observed in the spectrum or intensity of the measuring signal. By observing these changes, it is possible to obtain the value of measured quantity.

Many new materials have been successfully applied in the construction of fiber-optic biosensors, such as nanodiamond (NCD), boron-doped nanodiamond (B-NCD), zinc oxide (ZnO), titanium dioxide (TiO_2), and aluminum oxide (Al_2O_3). In this chapter, fiber-optic sensors, based on nanolayers or thin films as a protective coating, reflective layers and/or as a sensing medium, and their ability to perform biophotonic measurements is presented.

14.2 Fiber-Optic Sensors with Carbon-Based Nanolayers

14.2.1 Materials (NCD/XDND)

Diamond growth process and in situ doping depend on the manufacturing process parameters: substrate temperature, the composition of the working gases, the admixture of methane, or the degree of excitation of the plasma. Boron-doped diamond technology was developed by Shiomi *et al.* and confirmed by Spitsyn *et al.* (Shiomi et al., 1991; Spitsyn et al., 1981). Boron is the lowest level dopant, which can be incorporated into the diamond lattice with the energy level of 0.37 eV above the valence band level (Kalish, 1999; Wurzinger et al., 1997). The B_2H_6 (diborane) or $B(CH_3)_3$ (trimethyloborane) can be used as doping gas precursors. During the PA CVD synthesis from a mixture of CH_4/H_2 and gas activation, the two most common techniques to synthesize boron-doped diamonds (BDDs) are hot-filament CVD (HF-CVD) (Fabisiak et al., 2010) and microwave plasma-assisted CVD (MW PA CVD) in situ doped with boron precursors (Brillas and Martínez-Huitle, 2011). The boron dopant density, achieved by using MW PA CVD, ranges from 10^{16} to 10^{21} atoms cm^{-3} and *p*-type semiconducting materials transform to semimetal for the dopant density at 2×10^{20} (Fabisiak et al., 2010).

The BDD is currently one of the most effective semiconductor materials for electrochemical applications (Nebel et al., 2007). This material is characterized by a wide electrochemical potential window, chemical inertia, low current background (McCreery, 2008), and high biocompatibility (Stavis et al., 2011). Furthermore, this type of material is a thick-film BDD (approx. $5-10$ μm) having high absorption of optical radiation.

The growth diamond in the PA CVD on nondiamond substrates is ineffective and must be induced by a special treatment of substrates prior to using NCD powders, metal

nanoparticles, or surface roughness. This treatment is called "seeding" and may be implemented in several ways (e.g., mechanical abrasion, cavitation, ultrasonic treatment, wet etching, etc.). The most effective growth of BDD structures on such substrates can be obtained by carrying out the processes of seeding with NCD powders produced by the detonation method. To obtain a high adhesion and effective growth, the high density of substrate seeding (10^{11} cm^{-2}) has to be provided.

Finally, the substrates are pretreated in hydrogen plasma and seeded with the use of NCD suspension by spin-coating or dip-coating system to achieve highly conductive BDD structures with a low coefficient of absorption of optical radiation. Suspensions-based NCD dimethyl sulfoxide (DMSO) was mixed with polyvinyl alcohol (PVA). Mixed suspension DMSO-PVA has a higher viscosity, which allows for producing a thin seeding layer by spin-coating or dip-coating methods on the nondiamond substrates. The seeding process included immersing the fiber-optic twice for 1 min in the suspension. The automatic dip-coating mechanism was applied for these purposes (Fig. 14.1a).

The fiber-optics underwent hydrogenation in microwave H$_2$ plasma at 1300 W for 60 min. The introduction of pretreatment of the substrates of quartz glass in a microwave hydrogen plasma was performed. This process modifies the zeta potential of surface and significantly increases the density of seeding, which leads to an improved kinetics of diamond nucleation in the PA CVD (Bogdanowicz, 2014).

In order to investigate the influence of dip-coating seeding on diamond growth, we prepared a single-mode fiber-optic (cleaved Corning SMF28, cladding diameter of 125 μm, approx. 10 cm in length) where the polymer coating was mechanically removed. Deposition of conformal diamond films was demonstrated on fused silica fibers improved by hydrogen
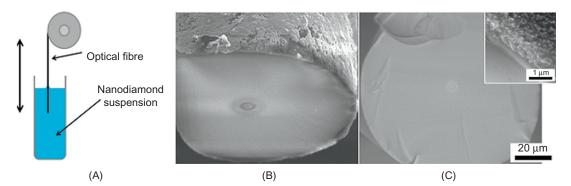

Fig. 14.1

Scheme of the automatic procedure for dip-coating (A); SEM micrographs of fiber cross section for nonhydrogenated (B) and hydrogenated (C) fibers. Magnification is 1000 ×. Insert: SEM image showing diamond coating (magnification 20,000 ×). *Reproduced with permission from Ref. (Bogdanowicz et al., 2014). Copyright 2014, Springer.*

plasma pretreatment and seeding in PVA-DMSO NCD suspension with dip-coating method (Fig. 14.1C) contrary to nonhydrogenated fibers (Fig. 14.1B). Moreover, the growth parameters were optimized resulting in low temperature growth of NCD films on 10 cm-long sections of fiber-optics, which could be used in sensing devices. Longitudinal research has shown that up to 5 cm in length of the fiber can be coated with uniform nanocrystalline structure and high sp^3 phase content.

These improvements of diamond structures make it an interesting material for the construction of the optoelectronic sensors. Considering the literature, electro-optosensing experiments require low resistivity (below 1 kΩ cm) (Zhou and Zhi, 2009) and high transmittance (over 50%) of the doped diamond sensing structures (Bosch et al., 2007; Stotter et al., 2002). These unique characteristics and the requirements can be achieved by overcoming challenging technological barriers.

The morphology of the surface of the samples was investigated by SEM (Fig. 14.2A). Subsequently, the transmission of radiation through the BDD structure in the VIS-NIR wavelength range (Fig. 14.2B) has been identified.

The resulting conductive BDDs have a high refractive index, low surface roughness (to minimize scattering of optical radiation), and a relatively low coefficient of absorption in the wavelength range Vis-NIR. Parameters of conductive BDDs (green) used for opto-electrosensing applications are summarized and compared with literature data (black) in Table 14.1. Stotter et al. (Stotter et al., 2003) enhanced boron-doped diamond electrodes to spectroelectrochemistry studies in the UV wavelength region showing good transparency at
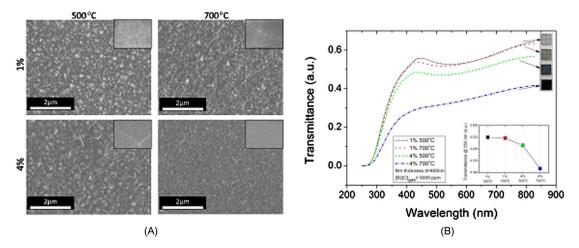

Fig. 14.2

SEM images of the surface of BDD structures (A) and the transmission of radiation through the structure (B), depending on the level of methane and the temperature of the substrate. *Reproduced with permission from Ref. (Bogdanowicz, 2014). Copyright 2014, De Gruyter.*
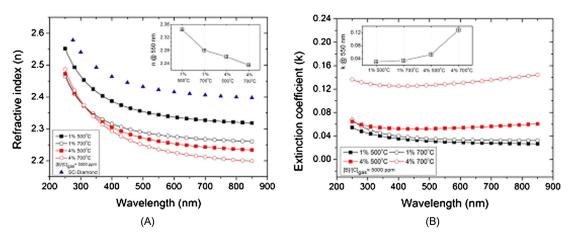
Table 14.1: Comparison of Transparent Conductive BDD Deposited on the Fused Silica Substrates

Structures BDD	Conditions T_s /CH_4	[B]/[C] [ppm]	Transmittance @ 550 nm [%]	Resistivity [Ohm cm]	Thickness [nm]	Reference
BDD-1-700	700°C/1%	5000	60	0.42	∼400	(Bogdanowicz, 2014)
BDD-4-700	700°C/4%	5000	30	0.02	∼360	(Bogdanowicz, 2014)
MCD	800°C/0.5%	10 of total	25	0.026	1000	(Stotter et al., 2002)
B:NCD/ NCD	500°C/1%	3000	60 (undoped)	40	400	(Williams and Nesládek, 2006)
B:NCD/ AlN/ITO	700°C/2%	3000	80	50 − 60	400	(Zuerbig et al., 2013)
B:NCD	700°C/1%	10,000	70	207	150	(Yeap et al., 2014)

50%−60%. Mermoux *et al.* (Mermoux et al., 2002) used confocal Raman imaging to study OTEs for samples with a thickness of 380 μm. Remes *et al.* (Remes, 2010) investigated the optical properties of undoped NCD film on fused silica by using photothermal deflection spectroscopy, calorimetry, and dual-beam photocurrent spectroscopy. Kromka *et al.* (Kromka et al., 2008) investigated the impact of low-temperature MW CVD process on optical properties of nanocrystalline diamond films (NCD) on silicon and quartz substrates; the films displayed a transmittance of ca. 70% and a high refractive index of 2.34 at 550 nm of wavelength. Potocky *et al.* (Potocky et al., 2007) showed a refractive index of 2.2−2.4 (at 550 nm) on quartz substrate for growth temperature below 400°C. The optical properties of diamond layers strongly depend on deposition temperature (Hu et al., 2007; Hu and Hess, 2006).

Spectroscopic ellipsometric study of optical parameters of BDD layers makes it possible to determine and optimize the optical absorption of doped layers. It should be noted that the undoped layers of nanocrystalline diamond have low optical attenuation. Described variations of BDD structures result from the process conditions and the gaseous precursors. In order to reduce the particle size, a higher percentage of methane was introduced to a standard mixture of CH_4/H_2. Moreover, the increase of seeding density using the NCD suspension mixed with polyvinyl alcohol (DMSO-PVA) was applied.

The refractive index varied between 2.24 and 2.35 for different methane contents and deposition temperatures at a wavelength of 550 nm (see Inset of Fig. 14.3A). The obtained values were smaller than those for the single-crystal diamond (2.41), which is related to a decrease in the sp^3/sp^2 carbon phase ratio. Most likely, the diamond film samples contained more defects and some nanocrystals. It was identified that the increase in the methane

Fig. 14.3

Wavelength-dependent variability of refractive index *n* (A) and extinction coefficient *k* (B) in BDD films deposited under various conditions related to methane admixture and the substrate temperature. For comparative purposes, the refractive index measurements for a single-crystal diamond are shown (▲-SCD). Insets: the variability of *n* and *k* measured at 550 nm. *Reproduced with permission from Ref. (Bogdanowicz, 2014). Copyright 2014, De Gruyter.*

content in the plasma and the higher temperature of the substrate, lower the refractive index of layers. The extinction coefficient shows diametrically opposed changes. The highest extinction coefficient *k* got a high methane content and high temperature substrate (see Fig. 14.3B). The aim of the experiment was to minimize the coefficient of absorption, which is directly proportional to the extinction coefficient. Therefore, it can be concluded that the lowest absorption ($k = 0.04$) have samples synthesized with 1% methane at a temperature of 500°C. The level of absorption is low and fully acceptable from the point of view of structures made for optical applications.

According to developed processes and procedures, continuous thin polycrystalline BDD electrodes are deposited on substrates of silicon, glassy carbon, titanium, and quartz glass with a diameter of 5−50 mm. Other substrate materials necessitate additional studies to optimize the synthesis process.
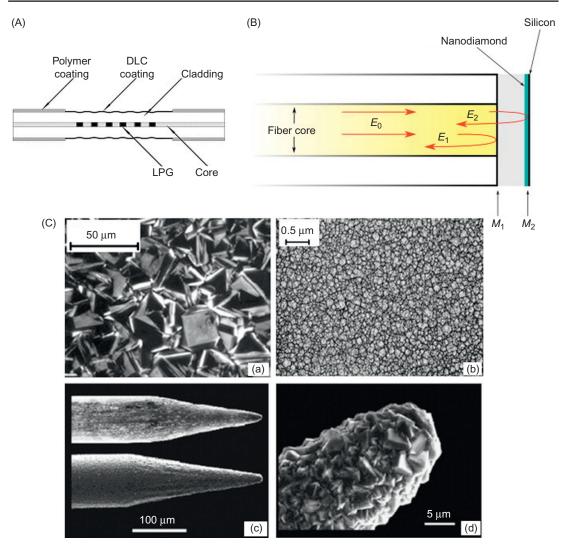
14.2.2 Electro-Optic Biosensing Applications

Diamonds are valued for their unique properties. In science and technology, the diamond is known for remarkable properties such as high thermal conductivity (Sukhadolau et al., 2005), mechanical hardness, optical transparency in broad wavelength (Checoury et al., 2012; Stotter et al., 2003), or biocompatibility (Amaral et al., 2008; Bajaj et al., 2007). Natural diamond is a wide band gap semiconductor with $Eg = 5.45$ eV, but can be doped with boron dopant in situ in chemical vapor deposition (CVD) and becomes *p*-type

semiconducting material (Bogdanowicz et al., 2013; Gajewski et al., 2009). BDD is widely used in electrochemistry due to outstanding properties like wide electrochemical window (Iniesta et al., 2001) and chemical stability even in hazardous media (Swain et al., 1998). It is a promising material to build organics (Choi et al., 2010), chemical, or biological sensors (Amaral et al., 2008; Bajaj et al., 2007). Moreover, due to its wide electrochemical window, it is a great material for electrodes for wastewater treatment. Furthermore, BDD film can be used as coatings for optical sensors or optically transparent electrodes (Sobaszek et al., 2016; Stotter et al., 2003).

Chemical measurements using fiber-optic gain a lot of interest due to the need for monitoring environmental pollution, industrial processes, and new technologies used in medical diagnostics. The demand for small, precise, and integrated measuring systems can provide long-period gratings. They are characterized by a periodic change in the refractive index inside the fiber-optic core. The thin diamond-like carbon (DLC) has significantly changed the characteristics of fiber-optic sensors. They have unique properties such as hardness and resistance to chemical destruction. The thin DLC sensor has shown high sensitivity to changes in the refractive index of various chemical solutions (Smietana et al., 2007). The proposed system, using DLC-protected long-period grating, gives a quick response and the ability to work continuously (Figure 14.4a). In addition, DLC coatings have been tested for biocompatibility, mechanical stability with biological liquids, and corrosion resistance. They have been used as corrosion protection coatings in the electronic industry (Wu et al., 2017), such as NdFeB permanent magnets. The measurements showed that the corrosion resistance in 3.5% NaCl and 5 mM H_2SO_4 was improved by the DLC coating. Also, the possibilities of their use in medicine as stents and guides were explored (Maguire et al., 2005). High mechanical tensile and compression forces severe limitations on the use of DLC-coated stainless steel. Silicon doping and the use of hydrogenated amorphous silicon interlayer (a-Si: H) minimizes the risk of cracks. The Si insertion reduced the film hardness and significantly improved corrosion barrier properties. The DLC silicon coatings stimulate less inflammatory activity than uncoated materials.

The undoped diamond can be used to modify the electrodes for biological or chemical measurement. Glass-carbon electrode modification allows for the direct measurement of hemoglobin (Zhu et al., 2007). Undoped diamond enhances the electron transfer process between protein molecules and electrode. The modified diamond electrodes have better stability of measurements. Undoped diamond can be used to modify the gold electrode allowing selective detection of glucose (Zhao et al., 2006). A glucose biosensor was based on covalent immobilization of glucose oxidase on undoped diamond-coated gold electrode. The effect of electrochemical anodization on diamond film was investigated. The electrochemical analysis of glucose was effectively conducted in the attendance of interfering agents such as ascorbic acid or uric acid. The construction of selective and sensitive glucose biosensors was possible thanks to the coating of the electrode with a diamond layer.

Fig. 14.4

Application and characterization of diamond structures: (A) The long-period gratings structure with a diamond-like carbon coating. Reproduced with permission from Ref. (Smietana et al., 2007). Copyright 2007, Elsevier. (B) Extrinsic FPI working in reflective mode: M1, M2—cavity mirrors, E0—the amplitude of an electric vector of an incident wave; E1, E2—the amplitudes of an electric vector of waves reflected from the first and second mirrors, respectively. Reproduced with permission from Ref. (Milewska et al., 2016) Copyright 2016, Elsevier. (C) The SEM images of BDD electrodes: (a) polycrystalline BDD thin film, (b) nanocrystalline BDD thin film, (c) electrochemically sharpened Pt wire (top) and a Pt wire covered with a polycrystalline BDD film (bottom), and (d) the tip of a 76 μm Pt wire covered with a BDD film. *Reproduced with permission from Ref. (Zhou and Zhi, 2009). Copyright 2009, Elsevier.*

The BDD film is used as electrode material. They have been used in amperometric biosensors which are characterized by high sensitivity, selectivity, repeatability, and high stability. They can be used as a glucose sensor, whose reliable, selective, and fast measurement is important for diabetics (Fig. 14.4c). The classic solution with glucose oxidase is characterized by high selectivity, but it is unstable. Electrodes made of metals such as gold or platinum allow glucose oxidation, but the problem is the presence of other components such as ascorbic acid (potential similar to glucose). BDD electrodes allow for the direct detection of glucose without the need for enzymes or metallic catalysts (Zhou and Zhi, 2009). Diamond film exhibits optical transparency from ultraviolet to far infrared. They are interesting materials for optically transparent electrodes that can be used for spectroelectrochemical measurements of various substances. They can be used for chemical detection and utilization of hazardous organic components (Sobaszek et al., 2016). UV-C anodes with a BDD film have been used to degrade coumarin, which is a component of many products, such as soaps or cosmetics (Montanaro et al., 2017). Due to high consumption, sustainability, and harmfulness to the environment, a degradation method should be developed. The effectiveness of the presented method was assessed on the basis of the reduction of coumarin concentration and disappearance of organic carbon. The research has shown that effectively coumarin degradation is possible on electrochemical oxidation on BDD anodes and UV irradiation. Additionally, diamond electrode with modified polymelamine showed good oxidation properties of adenine and guanine (Niedziałkowski et al., 2016). Adenine and guanine are the basic building blocks of nucleic acids (DNA and RNA). Protein detection was based on the process of their oxidation. The polymelamine-modified boron-doped electrodes showed good oxidative properties of the examined substances. They are very sensitive to the detection of guanine, adenine, and caffeine. The electrochemical method is useful for the determination of purines. Electrodes and silver needles were also used for electrochemical pH measurement in the diagnosis of gastric disorders (Fierro et al., 2013). The pH disorders may be related to malignant tumors, because cancer cells cause environment acidification. A change in the pH in cells has an influence on the deterioration of the antineoplastic agent. The electrodes combined with chronopotentiometry allowed pH measurements of the mouse's stomach. Precise pH calibration curves have been obtained. Developed electrode can be used in biological environment.

Undoped and boron-doped diamond films can be used as a mirror in low-coherence fiber-optic Fabry−−Pérot interferometer (FPI) (Milewska et al., 2016). The low-coherence measuring system is dedicated to measure the broad range of physical and biochemical quantities. The experiment setup consisted of optical spectrum analyzer, superluminescent diodes, and coupler. All elements were joined with standard telecommunication fiber-optic. The studies have been conducted for the low-coherence FPI working in reflective mode (Figure 14.4b). The cavity mirrors M_1 and M_2 used Fresnel reflection at the boundary between the single-mode fiber-optic and the surrounding medium as well as the surrounding

medium and diamond film. Application of diamond films in fiber-optic interferometers as a reflecting layer improved the visibility values (*V*). The results have shown successful integration in sensing applications. Additionally, the fiber-optic low-coherence FPI with thin boron-doped or undoped diamond film and thin ZnO layer as reflective surface was investigated (Majchrowicz et al., 2016a,b,c). Two wavelengths (1290 and 1550 nm) were used for measurements of the metrological properties of the interferometer. The use of the diamond mirror in the construction adds tolerance to the environmental conditions. The achieved results show that diamond film provides good visibility of the interference signal and therefore it can be successfully integrated in sensing devices. The interferometer can be the base for building new configuration sensors of physical quantities.

14.3 Fiber-Optic Sensors with Noncarbon-Based Nanolayers

14.3.1 Materials (TiO2, ZnO)

Recently, a wide range of thin film deposition methods was developed and opened the route for the design of new class of materials such as thin films, nanostructures, and nanocomposites. Among these methods, atomic layer deposition (ALD) has attracted a lot of attention due to its ability to design ultrathin films of inorganic materials and to control their thicknesses at subnanometric level (Marichy et al., 2012).

ALD can be employed to coat complex substrates and nanomaterials with conformal and uniform ultrathin films. These properties make the ALD technique unique among the different thin film deposition methods. The materials designed by ALD could be applied in various fields of energy (osmotic power, hydrogen purification, and fuel cells) (Drobek et al., 2015; Le et al., 2016), health (cell proliferation, DNA sequencing, and controlled drug delivery) (Cabello-Aguilar et al., 2013), and environment (sensors, biosensors, and purification of water by photocatalytic effect or electro-Fenton process (Drobek et al., 2016; Le et al., 2017)).

ALD is a vapor phase deposition method. It is based on self-limiting reactions taking place at the surface of the substrate in a cycle-wise manner. A typical ALD cycle consists of alternate pulses of a precursor and coreactant gasses in the reactor chamber, separated by purge steps. The properties of the synthetized thin films and nanomaterials can be controlled by tuning different parameters such as the process conditions (chemistry of the precursors and the coreactants), the temperature, the number of cycles, and the nature of the substrate (Marichy et al., 2012). Although ALD is typically used for the synthesis of oxide thin films, nitrides and metals have also been deposited using this method. Recently, we investigated the applications of thin oxides (zinc oxide (ZnO) and TiO2) in ALD layers in fiber-optic Fabry−Pérot sensing interferometers (Hirsch et al., 2017; Jędrzejewska-Szczerska et al., 2015; Majchrowicz et al., 2016a,b,c).

ZnO is a highly potential *n*-type semiconductor with many promising properties, i.e., transparent conductive oxide (TCO) of excellent optoelectronic proprieties, a wide band gap (3.36 eV), high dielectric constant, high exciton binding energy (60 meV), and high thermal stability. ZnO was used for a wide range of applications such as gas sensors, biosensors, solar cells, and transparent electrodes. The optoelectronic properties of ZnO thin film are well known to be strongly dependent on different parameters such as the morphology, the crystallinity, and the chemical composition. Jędrzejewska-Szczerska et al. reported on optical fibers with ZnO thin film used for temperature measurement. The sensor employs low-coherence interferometry technique to interrogate a Fabry−Pérot sensing interferometer formed by ZnO thin film (310 nm) deposited by ALD on fiber tip (Jędrzejewska-Szczerska et al., 2015). Majchrowicz et al. (Majchrowicz et al., 2016a,b,c) studied the metrological parameters of the fiber-optic FPI with thin ZnO layers of different thicknesses deposited using ALD on the end faces of the single-mode optical fiber which form the mirror of Fabry−Pérot cavity.

As an example of these ZnO ALD layers, Fig. 14.5 shows the chemical and optical properties of 310 nm ZnO films deposited by ALD. Fig. 14.5a shows the SEM images of ALD ZnO thin films deposited on Si substrates with 1250 cycles indicating a conformal coating of the Si substrate. The ZnO films show a columnar growth with a rough surface. GIXRD diffraction (Fig. 14.5b) shows peaks at $2\theta = 31.74°$, $34.42°$, and $36.22°$ corresponding, respectively, to (100), (002), and (101) of ZnO. AFM image of ZnO film is shown in Fig. 14.5c. The sample showed good polycrystalline structure with well-shaped nanograins. The average size of the nanograins was $40 − 60$ nm. The surface roughness value (rms) was 2.82 nm. Transmittance spectra of ZnO layer is shown in Fig. 14.5d. The samples were transparent in the range of wavelengths $440 − 1100$ nm. The absorption edge of the ZnO film at $340 − 440$ nm is typical for ZnO nanostructures. The band gap of ZnO film calculated using the optical density was 3.28 eV (Fig. 14.5e). Room temperature photoluminescence spectrum of ZnO is shown in Fig. 14.5f. Two emission bands in UV and visible range are observed. The analysis of the spectrum performed by Origin software showed single peak positions. The peaks in UV region at 3.3, 3.25, and 3.16 eV correspond to free (FX), bound (D0X) excitons, and the phonon replica, respectively. The peaks at visible range at 2.24 and 1.9 eV correspond to the structural defects: oxygen vacancy and interstitial oxygen, respectively.

Hirsch et al. (Hirsch et al., 2017) reported the application of TiO2 thin film in low-coherence fiber-optic biosensors. TiO2 has drawn the maximum attention due to its relatively low cost, high stability, and low toxicity. TiO2 has been widely used in many applications including dye-sensitized solar cells, gas sensors, biofuel cells and biomaterials, as well as photocatalytically active nanoparticles (Sarkar et al. 2012) and gypsum-titania fiber nanocomposites for indoor antimicrobial coatings (Mohl et al., 2014).
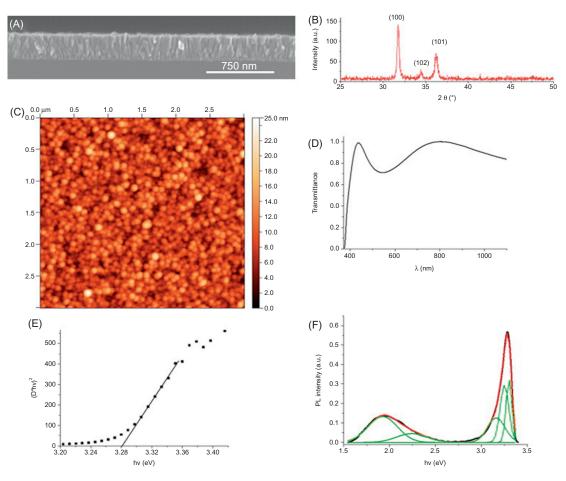
Fig. 14.5

(A) SEM cross-section image of ZnO ALD films deposited on Si substrates with 1250 cycles, (B) GIXRD, (C) AFM image, (D) transmittance spectra, (E) band gap calculation of ZnO film, and (F) room temperature photoluminescence spectrum of 310 nm ZnO film. *Reproduced with permission from Ref. (Ję̨drzejewska-Szczerska et al., 2015). Copyright 2015, Elsevier.*

TiO2 films with the thickness of 80 nm have been deposited on the tip of a single-mode optical fiber by ALD. The thickness, the structure, and the chemical properties of the films have been determined. ALD of TiO2 was achieved using sequential exposures of (iPrO)4Ti and H2O at 120°C. In order to achieve the deposition of ∼80 nm TiO2, 4000 ALD cycles were carried out. Interestingly, it has been shown in previous studies that the amorphous, anatase, and rutile phases of TiO2 can be obtained by tuning the ALD process parameters, and that the films with different crystallinity phases presented different optical and photocatalytic properties.

Chemical and structural characterizations of an example of TiO2 thin film deposited by ALD have been performed and showed in Fig. 14.6. Fig. 14.6a shows the SEM image of an
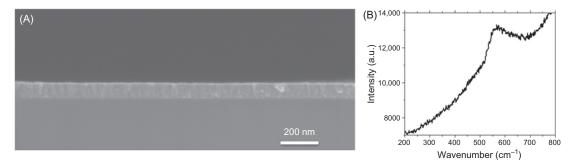
Fig. 14.6

(A) SEM cross-section image of TiO2 films deposited by ALD on Si substrates and (B) Raman spectrum of TiO2 films deposited by ALD. *Reproduced with permission from Ref. (Hirsch et al., 2017). Copyright 2017, MDPI.*

ALD-grown TiO2 film deposited on Si substrate. The conformal coating of the Si substrate by the ALD TiO2 film can be clearly seen. Spectroscopic ellipsometry (SE) measurements were carried out to evaluate the TiO2 film thickness as well, and for this specific sample, a thickness of 82 ± 2 nm has been obtained. Grazing-incidence XRD measurements have been realized and the absence of peaks in the spectra obtained suggested that the as-deposited TiO2 film at 120°C was amorphous. The formation of the amorphous TiO2 phase was further confirmed by Raman spectroscopy (Fig. 14.6b), since the Raman spectra of the deposited TiO2 films did not show any peaks either.

This result is in agreement with previous studies that showed that TiO2 films deposited by ALD below 120°C are amorphous, and that annealing at temperatures above 300°C are typically required to obtain the crystallization of the films. Crystalline TiO2 typically exhibit the anatase phase, but the rutile phase can also be achieved by ALD, using ozone or plasmas as coreactants. The relative density of the ALD TiO2 has been reported elsewhere to be 3.6 g/cm^3. Finally, the biosensing properties and the stability of the presented sensor have been verified, showing the potential of ALD thin films prepared on FPI.

14.3.2 Fiber-Optic Biosensing Applications

Integration of thin films allows designers to achieve high sensitivity of the fiber-optic biosensors and to perform label-free measurements. In general, the biosensing fiber-optic systems can be realized on the base of direct sensing—by measuring the properties of the transducer sensitive to bio-derived quantities, for example, refractive index. Among the most popular methods are reflectometry, interferometry, ellipsometry, and surface plasmon resonance (SPR) (Tereshchenko et al., 2016). There are also sensors based on the indirect sensing techniques, where the measurements are performed for detection of change in the attached tag that reacts to target analyte (e.g., fluorescent tags) (Tereshchenko et al., 2016).

Titanium oxides exhibit a number of features that predestine it for use in optical biosensing: low absorption in the VIS-NIR light, high refractive index, chemical stability and durability, and, most of all, biocompatibility. Moreover, the surface functionalization for selective molecule binding can be successfully applied to thin TiO_2 films (Dominik et al., 2017). Due to those, the TiO_2 thin films are widely used in various configurations of the optical biosensors. The existing schemes utilize the thin films to fine-tune the device sensitivity for biosensing measurements but also as a selective biointerface layer with surface biofunctionalization applied (e.g., for detection of proteins or enzymes).

One of the fields where TiO_2 thin films find use is SPR-based sensors. The principle of operation in such sensors is based on the excitation of a surface plasmon on metal−dielectric interface stimulated by the incident light. Most commonly, the detection in SPR fiber-optic sensors is realized by measurements of transmission loss at the resonance wavelength. The variation in refractive index of the investigated sample results in a shift of the resonance frequency (Klantsataya et al., 2016).

SPR-based sensors are broadly used in biosensing (Klantsataya et al., 2016; Pospíšilová et al., 2015; Wang and Wolfbeis, 2016). In most of the applications, the surface needs to be functionalized with bioreceptors (e.g., antibodies, enzymes, proteins) to achieve the selective interaction with investigated analyte (Dominik et al., 2017; Klantsataya et al., 2016). However, during the process of biofunctionalization, there is a risk of corruption of the metal layer—for example, in case of the nanoparticles layer, some of them can be washed out during steps of the procedure (Dominik et al., 2017). Another issue is that the metal coatings are prone to oxidation, which influences sensitivity and resonance wavelength of the device (Singh et al., 2013).

It was shown that the application of a thin (13 − 14.5 nm thickness) titanium oxides film over a gold nanoparticles layer deposited on glass substrate in localized SPR sensor can improve its mechanical resistance and protect the metal layer. Such film was shown to be successfully biofunctionalized with biotin for avidin recognition. The achieved sensitivity was 30 nm/RIU (refractive index units) and observed shift in the resonance wavelength was 3 nm (Dominik et al., 2017).

Adjustments in thickness of the oxide layer and the optical parameters of deposited material can be used to fine-tune the sensitivity and the resonance wavelength of the SPR sensor (Dominik et al., 2017; Singh et al., 2013). The study of enhancement of the SPR refractive index (RI) sensor by use of additional oxides film shows that optimized selection of those parameters allows to obtain up to 2.5 times increase in sensitivity (Singh et al., 2013). The copper layer fabricated on the multimode plastic clad silica fiber was coated with TiO_2 film of various thickness (5, 7, 10 nm). The measurements were performed for the different sucrose concentrations (RI in the range 1.33 − 1.37). Comparison of the results obtained for

sensor with bare copper and with 10 nm TiO_2 overlay demonstrates the shift of the resonant wavelength from $630 - 710$ nm to $760 - 950$ nm, respectively, for the measured RI range (Singh et al., 2013).

It was observed that the addition of a thin TiO_2 layer results in a shift of the resonance toward the longer wavelengths. This effect can be utilized to move operation of fiber-based SPR sensors to the NIR wavelengths—the main advantage is working in the frequency bands common in telecommunication, hence a wide choice of the fibers and the electronic equipment is commercially available (Coelho et al., 2016, 2015). An example of such a design is aptamer-based fiber SPR sensor for thrombin detection (Coelho et al., 2016). It was fabricated by deposition of multilayer structure of 2 nm chromium, 16 nm gold, and 100 nm TiO_2 layers on the chemically etched single-mode fiber. The TiO_2 surface was fictionalized with poly-l-lysine (PLL) and then treated with the DNA probe for recognition of thrombin (TBA). The obtained wavelength shift for 10 nM concentration of thrombin was 3.5 nm and 5 nm for 50 nM (Coelho et al., 2016). However, for higher concentrations of the enzyme, the sensor reached the saturation limit. The operation range should be possible to expand by adjusting the PLL/TBA concentrations in the functionalization process (Coelho et al., 2016).

Also, in more elaborate fiber structures, like microstructured fiber-optics (MOF) (Gao et al., 2014) and multicore flat fibers (MCFF) (Rifat et al., 2016), the TiO_2 thin films deposited over the gold layers were effectively used to shift the resonance wavelength to the NIR range and to enhance the evanescent fields. The proposed sensors are operational in the $1300 - 1400$ nm wavelengths and achieve high sensitivity of the RI sensing—9600 nm/RIU in $1.460 - 1.485$ RI range was shown for the MCFF and 2000 nm/RIU in RI range $1.33 - 1.35$ for the MOF (Gao et al., 2014; Rifat et al., 2016).

The other domain where TiO_2 thin films find applications are sensors based on long period gratings (LPG). The LPG sensor is created by periodic modulation of RI in the core of a single-mode fiber. Usually, the period of grading is in the range of $100 - 700$ μm (Chiavaioli et al., 2017). Introduction of the periodic structure allows for coupling of light from the core mode into the discrete set of forward-propagating cladding modes. The result is a series of resonance attenuation peaks visible in the transmission spectra of the LPG. The wavelength of the resonance (λ^m) is dependent of the effective refractive index of the cladding ($n_{eff}^{clad(m)}$) and the core (n_{eff}^{core}) mode, as well as grading period (Λ) (Smietana et al., 2015):

$$\lambda^m = \left(n_{eff}^{core} - n_{eff}^{clad(m)} \right) \bullet \Lambda \qquad (14.7)$$

The RI sensing principle of LPG is based on dependence of the $n_{eff}^{clad(m)}$ on the RI of external medium. However, the best sensitivity is achieved when the value of the external RI is close to that of the cladding (typically made of fused silica, with RI ~ 1.458) (Chiavaioli et al., 2017; Smietana et al., 2015).

One way to adapt the LPG sensors to the RI range most common for measurement of the biochemical samples ($\sim 1.3 - 1.4$) is coating the sensor with a thin layer of material with higher refractive index than that of the cladding (Chiavaioli et al., 2017). The TiO_2 films proved to be an interesting choice for the application.
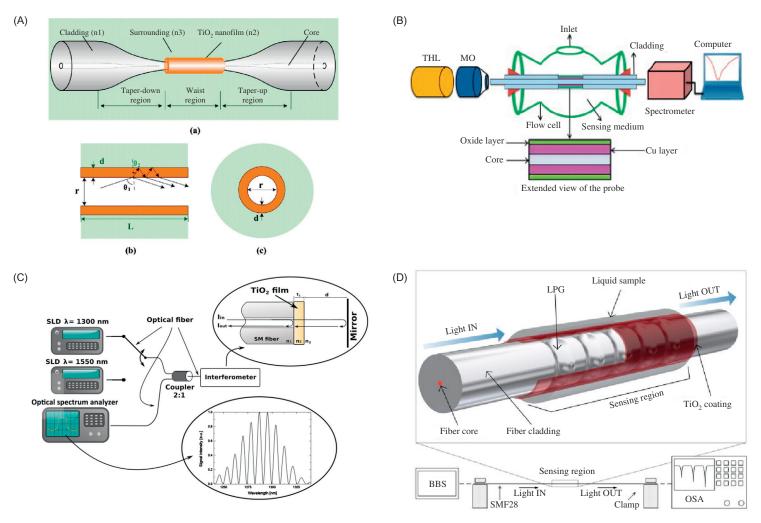
Śmietana et al. presented a study where they investigated the response of LPGs overlaid with TiO_2 layers of different thickness (Smietana et al., 2015). The most promising results for biosensing application were obtained for 70 nm overlay. Tuning of the thickness of TiO_2 layer allowed for operation close to dispersion turning point that resulted in very high sensitivity (6200 nm/RIU) for the RI up to 1.34. The sensitivity for RI up to 1.39 was also high, close to 3000 nm/RIU, making it well suitable for label-free detection (Smietana et al., 2015). The surface of the 70 nm TiO_2 film was biofuctionalized with bacteriophage adhesion and successfully tested for detection of bacteria lipopolysaccharide (Smietana et al., 2015).

The successful biofunctionalization of TiO_x films deposited on LPG was also performed with biotin (Dominik et al., 2017). The LPG sensor was coated with ~ 63.8 nm TiO_x layer by ALD. Before the biofunctionalization procedure, the sensitivity for RI measurements was determined as close to linear and up to 3400 nm/RIU for RI in the range $1.33 - 1.38$. Then, the TiO_x surface was functionalized with biotin. The results for the avidin bonding showed a shift of the resonance wavelength of 13.2 nm (Dominik et al., 2017).

The LPGs enhanced with thin TiO_2 film has been shown in a number of other biosensing applications (Chiavaioli et al., 2015; Coelho et al., 2016; Yang et al., 2012). An aptamer-based sensor for thrombin detection is an interesting solution, utilizing a fiber Bragg grating (FBG) for temperature compensation in addition to biofunctionalized LPG (Coelho et al., 2016). An antibody/antigen immunoassay (IgG/anti-IgG) was shown with use of TiO2−SiO2 layer coated on the LPG by sol-gel method (Chiavaioli et al., 2015). An enhancement of the LPG sensing properties in aquatics solutions by application of nanoporous TiO_2-Polyion thin overlay was used for measurements of low-molecular-weight analytes (e.g., low glucose concentrations) (Yang et al., 2012). {{{Figure 14.7}}}.

The TiO_2 thin films also find application in sensors based on reflectometry and interferometry (Hirsch et al., 2017; Pathak et al., 2017; Rozycki-Bakon et al., 2016; Zhu et al., 2016). In such solutions, the thin film is usually deposited on the fiber tip or on the tapered region of the fiber.

A specific example of fiber tip modification would be use of a nanocomposite, as was shown by Różycki-Bakon et al. (Rozycki-Bakon et al., 2016). The stack of TiO_2-Al_2O_3 nanofilms was deposited on the end-face of a single-mode fiber. The structure consisted of five layers: four alternate films of TiO_2 (132 nm) and Al_2O_3 (128 nm) and the external, slightly thinner (117 nm) TiO_2 layer. Such periodic nanostructure consisted of materials

Fig. 14.7

Applications of TiO$_2$ thin films in fiber-optic sensors: (A) Schematic diagram of (a) the tapered fiber coated with TiO2 nanofilm, and the coated region in the (b) axial and (c) radial directions. Reproduced with permission from Ref. (Zhu et al., 2016). Copyright 2014, MDPI. (B) Schematic of experimental setup for SPR-based fiber-optic sensor. Reproduced with permission from Ref. (Singh et al., 2013). Copyright 2013, Elsevier. (C) Schematic of experimental setup for the FPI. Reproduced with permission from Ref. (Hirsch et al., 2017). Copyright 2017, MDPI. (D) Scheme of the LPG sensing head and of the measuring setup. (BBS— broadband source, OSA—optical spectrum analyzer). *Reproduced with permission from Ref. (Coelho et al., 2014). Copyright 2014, Elsevier.*

with lower and higher RI can be considered a short Bragg grating with only two periods (Rozycki-Bakon et al., 2016). Sensor showed linear and temperature-stable response in the RI range $1.31 - 1.44$. Then, the surface of the external TiO_2 film was functionalized with biotin and tested, showing the ability to detect avidin presence in the sample (Rozycki-Bakon et al., 2016).

Another example of fiber tip modified design that can benefit from application of TiO_2 are cone-shaped sensors (Pathak et al., 2017). In the pH sensor, a thin TiO_2 film was deposited on chemically tapered, cone-shaped tip of multimode fiber. The pH sensing matrix was fabricated over TiO_2 layer. The principle of sensor operation is based on the total internal reflection at the tip boundary. The detection is performed through intensity interrogation of reflected light (Pathak et al., 2017). The application of TiO_2 film induced an enhancement of evanescent field at the glass$-TiO_2$ interface leading to visible improvement in sensor sensitivity (0.53 dBm/pH for uncoated probe, 1.1 dBm/pH for sensor with deposited TiO_2) (Pathak et al., 2017).

Integration of thin TiO_2 films was shown to be advantageous also in fiber-optic sensing interferometers. The most promising for biosensing application are constructions based on FPIs, as they achieve very high sensitivity in measurements of RI changes (Pluciński and Karpienko, 2016). However, the reflective plane of the interferometer is usually created by boundary of the fiber tip and the external medium. When the RI of surrounding medium is close to that of a fiber, the reflectivity of the boundary is low. It results in poor contrast of interference fringes that in turn sets a higher requirement for the detector and can lead to potential errors in noisy environments. Deposition of a high refractive index thin interface layer, like TiO_2 film, can be used to fine-tune the reflectance of the fiber-cavity boundary, and thus the finesse function of the FPI, for operation in the RI range suitable for biosensing (Hirsch et al., 2017).

Such enhancement by deposition of a thin TiO_2 film on the end-face of a single-mode fiber was proposed for low-coherence FPI (Hirsch et al., 2017). The adjustment of thickness and RI of the layer can be used for tuning of the film effective reflectance. However, choosing the optimal value has to be performed with care, as with TiO_2 an effect of interference in the layer strongly influences the spectral reflectance function of the film (Hirsch et al., 2017, 2016). In the low-coherence FPI, the 80 nm TiO_2 film was deposited by ALD on a clean-cut fiber tip. The application of the additional layer allowed for improvement of the visibility of interference pattern, especially for the short cavity length (50 μm). Good visibility of the interference signal was maintained during the measurements of glucose concentrations and hemoglobin (Hirsch et al., 2017).

The thin TiO_2 film—treated as a Fabry$-$Pérot cavity—was also used in sensitivity improvement of a refractometer based on tapered single-mode fiber (Zhu et al., 2016). The TiO_2 layer was deposited over the waist region of the taper and the interference in thin film

formed an attenuation band in NIR transmission spectra. The changes in RI of surrounding media result in a shift of the resonance wavelength. Influence of the film thickness (39.7, 45.2, and 50.9 nm) was examined to optimize performance for operation in RI range close to water (Spitsyn et al., 1981). The increase of TiO_2 overlay thickness caused movement of the resonance dip toward longer wavelength and also increase of the shift induced by external RI changes (Zhu et al., 2016).

The integrated photonics structure based on planar waveguide are widely applied, among others, as a waveguide, optical modulators of light, optical filters, as well as optical sensors structure. Of special interest are optical biosensors based on integrated photonics structures for biomedical applications. The key issue of optical biosensors based on integrated photonics structures are: principle of operations, materials applied as a waveguide layer and sensor layer, as well as the way which light is coupling into the structure and uncoupling from the waveguide structure.

The integrated photonics structure for biosensors applications is built in the form of planar waveguide which consists of: waveguide layer (refractive index n_w) with an additional sensor layer—chemically selective layer (refractive index n_{ss}), these layers are deposited on substrate (refractive index n_s). The scheme of the sensor structures are presented in Fig. 14.8a and Fig. 14.8b. The analysis of literature indicates the integrated photonics
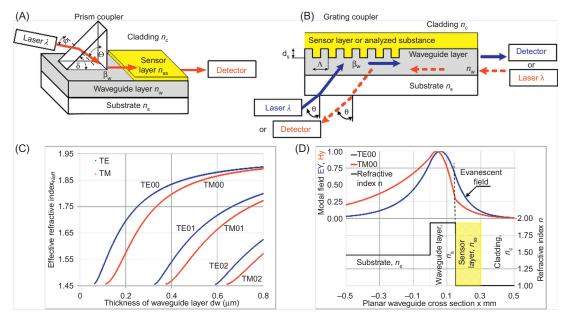

Fig. 14.8

The scheme of biosensors based on integrated optics: (A) structure with prism coupler, (B) structure with grating coupler, (C) modal characteristic of waveguide, (D) distribution of modal field in waveguide layer. The additional sensor layer was marked by yellow color.

structure for biosensors applications works mostly based on evanescence field of guided waveguide mode (Lukosz, 1995; Mukundan et al., 2009). The evanescence field of guided waveguide mode penetrates and "scanning" the surrounding layers: cladding or sensor layer (evanescence field in the substrate layer is negligible from the sensor point of view) (Binghui and Heongkyu, 2013). The changes of optical or geometric properties of sensor or cladding layer affects changes of propagation conditions of waveguide modes and can be detected in sensor structures. The waveguide structure and its optical and geometrical properties of each layer can be described in quantity by effective refractive index N_{eff} (Lukosz and Tiefenthaler, 1988). The effective refractive index of guided waveguide mode depends on the optical and geometrical properties of waveguide structure such as: refractive index of substrate, waveguide, sensor and cladding layer, and its thickness, wavelength, and polarization of light (Lukosz and Tiefenthaler, 1988). The analysis of literature indicates that in biosensors structures, the effective refractive index N_{eff} can be changed mostly in the following ways:

- creation of an additional layer on waveguide layer by adsorbed, bound molecules of liquids or gas—the effective refractive index of guided mode in waveguide is changed by refractive index of additional layer and its thickness (Lukosz, 1995);
- changes of optical properties (refractive index) and geometrical properties (thickness) of sensors layer deposited on waveguide layer (Lukosz and Tiefenthaler, 1988; Tiefenthaler and Lukosz, 1989);
- changes of optical properties of cladding or sensor layer (refractive index of layer, effective refractive index) in the range of grating coupler (Vörös et al., 2002).

The examples of effective refractive index N_{eff} as a function of waveguide layer thickness d_w as well as modal field distribution in planar waveguide is presented, respectively, in Fig. 14.8c and Fig. 14.8d. The figure presents also evanescence field for TE00 and TM00 modes, the border between waveguide and cladding layer is marked by a dashed line. The presented modal field distribution was calculated for single-mode waveguide with following optical and geometrical parameters: substrate—quartz $n_s = 1.456$, waveguide—150 nm of ZnO $n_w = 1.933$, cladding—air $n_c = 1$, wavelength $\lambda = 677$ nm. The evanescence field of guided waveguide mode can also be applied in biosensors for measurements of absorbance changing of sensors layer deposited on waveguide under influence of external environment (Puyol et al., 2005).

The key issue in integrated optics biosensors structure is the way which the light beam generated by the laser is coupled into waveguide layer with thickness at the level from several hundred nanometers to several micrometers. The technical solution of input−output system for coupling of the light beam into planar waveguide should be of high efficiency, easy for applications, and repeatable, in addition—not to make significant changes in the geometrical dimensions of the integrated optical structure. The most popular way for

coupling of the light beam into waveguide structure is: prism coupler or grating coupler. The schematic view of prism coupler is shown in Fig. 14.8a. The collimated light beam generated by the laser falls on the prism at an angle φ. Next, the light beam propagates into prism illuminates the base of the prism at an angle Θ. The introduction of light into the waveguide structure occurs in the range of the optical contact between the prism and waveguide layer by the effect of tunneling of light. The tunneling of light into the waveguide layer and excitation of waveguide occurs when the components of the wave vector along the way of propagation in the prism and waveguide layer are the same, and corresponds of the propagation constant in the waveguide layer (Struk et al., 2013; Pustelny and Struk, 2012).

The coupling condition of light into waveguide structure by prism coupler defines the equation (14.8) (Hunsperger, 2009; Lambeck, 2006). The angle at which the light beam is coupled into the planar waveguide is called the synchronous angle.

$$\frac{2\pi}{\lambda_0} n_p \cdot \sin\Theta = \beta_w = \frac{2\pi}{\lambda_0} N_{\text{eff}}, \tag{14.8}$$

where: n_p—the refractive index of the prism, Θ—the angle of incidence on the upper boundary plane of the waveguide, β_w—propagation constant in the waveguide, N_{eff}—effective refractive index of the waveguide mode, λ_o—wavelength.

The effective refractive index N_{eff} for the waveguide mode can be calculated concerning the synchronous angle of the equation (14.9) (Opilski 2002):

$$N_{\text{eff}}(\varphi) = \sin\delta \sqrt{n_p^2 - n_c^2 \cdot \sin^2\varphi} + n_c \cdot \cos\delta \cdot \sin\varphi, \tag{14.9}$$

where: n_p, n_c—refractive indices of the prism and cladding, δ—breaking angle of the prism, φ—angle of incidence of the light beam on the prism determined to normal.

The prism coupler is a useful tool for research of waveguide properties of planar waveguide structure (modal characteristic—value of effective refractive index for each waveguide mode) and for coupling of light into planar waveguide. However, the disadvantage of the prism coupler is that the final sensors structure is not planar but a spatial 3D structure. In addition, the prism have to be pressed to a waveguide layer by an additional mechanical system.

The photonics structure with grating coupler is an interesting technical solution, which permits the coupling or uncoupling of the light into or out of the integrated optics structure with thickness in the range of several hundred nanometers—several micrometers. In addition, the grating coupler can be the basis of operation of integrated biosensors structure. The grating coupler is constructed in the form of periodical disturbances of the refractive index on the surface of the waveguide layer (in the direction of light) with geometrical parameters such as: the so-called spatial period of the grating Λ, depth of grooves in grating

coupler d_s, their shape (Struk et al., 2013). The scheme of a photonic structure with grating coupler with marked waveguide layer n_w, sensor layer n_{ss}, substrate layer n_s, cladding layer n_c is shown in Fig. 14.8b. As already mentioned above, a photonic structure with a grating coupler can be applied as a light input − output system for the light. The coupling or uncoupling of light into or out of the structure by means of a grating coupler is marked, respectively, by the blue line and red-dashed line in Fig. 14.8b. The coupling of light into the integrated photonic structure or uncoupling from there by means of grating couplers is possible if the required conditions of matching the propagation constants in the environment and grating structure is met. The matching condition of propagation constant for grating coupler is presented in equation (14.10) (Lukosz and Tiefenthaler, 1988; Yariv and Nakamura, 1977).

$$\beta_c \bullet \sin(\theta) = \beta_w + \frac{m2\pi}{\Lambda}, \tag{14.10}$$

where: β_c, β_w—propagation constants in the environment and in the structure, respectively; Λ—spatial period of the grating, m—order of diffraction, θ—angle of the light beam incidence relative to the normal direction.

The principle of operation the grating coupler sensor is based on changing of the refractive index of cladding n_c (or sensors layer under influence of external environment) which causes changes of effective refractive index N_{eff} of guided waveguide mode in the region of grating (Tiefenthaler and Lukosz, 1989; Vörös et al., 2002). Any changes of the mentioned parameters (n_c and hence N_{eff}) in the range of grating coupler cause changes of the angle θ (equation (14.11)) (Bilitewski et al., 1998; Vörös et al., 2002). Transforming the equation (14.10), we get the dependence on the angle θ of the coupling or uncoupling the light into or out of the structure as a function of: refractive index of cladding, effective refractive index, diffraction order, and spatial period of the grating and wavelength (equation (14.11)) (Gartmann and Kehl, 2015; Pustelny and Struk, 2012):

$$\theta = \arcsin \frac{1}{n_c} \left(N_{eff} - \frac{m\lambda}{\Lambda} \right), \tag{14.11}$$

$$N_{eff} = n_c \bullet \sin\theta + \frac{m\lambda}{\Lambda} \tag{14.12}$$

The angle θ of the light beam incidence relative to the normal direction on grating coupler can be measured by dedicated measurement setup described, for example, in (Struk et al., 2009). An advantage of grating couplers is that they can be constructed as an integral part of the photonic structures. Thanks to this, the scale of integration and miniaturization of the completed structure can be enlarged. The grating coupler can be fabricated using a wide range of technology, for example: selective etching of waveguide layer (inductively coupled

plasma etching (ICP), reactive-ion etching (RIE)) or by embossing technology (Struk et al., 2011; Waldhäusl et al., 1997). The key issue is also the design of optical and geometrical properties of grating coupler (value of refractive index and thickness of each layer, spatial period Λ, depth of grating grooves d_s, and fill factor of grating grooves k) for optimization efficiency of coupling or uncoupling light into or out of the structure. The above-mentioned numerical analysis can be carried out, among others, by the finite difference time domain (FDTD) method (Pustelny and Struk, 2012). The literature indicated the application of grating coupler in the biosensors is, among others: measurement of binding interaction of IgG (Immunoglobulin type G) to antibody (Clerc and Lukosz, 1997) pesticide detection (Piehler et al., 1997), protein–DNA interaction (Vörös et al., 2002), and human b2-microglobulin detection (Brynda et al., 1999).

The key part of integrated photonics sensors structures based on planar waveguide is material used as a waveguide layer and sensor layer. The material used as a waveguide layer should meet several requirements, such as: a higher value of refractive index n_w than cladding n_c and substrate layer n_s, optically transparent for the light at the point of operation of the photonics structure, as well as the deposition technology on substrate should be easy, repeatable, and relatively cheap. The above-mentioned requirements can be met by selected semiconductor materials, in particular with wide energy band gap such as ZnO. The analysis of literature shows the ZnO semiconductor is transparent for the light in visible spectrum of light (absorption edge is at the level of $\lambda_{ZnO} \sim 370$ nm) (Struk et al. 2014; Özgür et al., 2005). The ZnO semiconductor is characterized also by a high value of refractive index at the level of $n_{ZnO} \sim 1.9$ depending on wavelength as well as deposition technology (Struk et al, 2014; Özgür et al., 2005). The ZnO semiconductor can be deposited on substrate in a wide range of technology methods (depending on application requirements) such as: electron beam evaporation (E-Beam), pulsed laser deposition (PLD), molecular beam epitaxy (MBE), CVD, and sol-gel method (Jagadish and Pearton, 2006). However, a very interesting deposition method of ZnO semiconductor is DC mode or RF mode reactive magnetron sputtering. The ZnO layer deposited by reactive magnetron sputtering can be characterized by relatively low surface roughness—the root mean square roughness (rms) is at the level of a few nm or less. This type of ZnO semiconductor can be applied as a waveguide layer in integrated optics structures. The planar waveguide structure-based smooth ZnO layer can be characterized by a relatively good waveguide properties such as: low attenuation coefficient of light for the waveguide modes at the level $\alpha \sim 3$ dB/cm (Struk et al., 2011; Heideman et al., 1995). On the other hand, the ZnO layer deposited by reactive magnetron sputtering method can be characterized by a developed surface with relatively high surface roughness, with rms at the level of tens of nanometers (Struk et al., 2015). Furthermore, the ZnO layer deposited by reactive magnetron sputtering can take a porous structure (Struk et al., 2015). The high surface roughness, porous

structure, or nanostructures of ZnO layer is desirable properties especially in sensor structures, for example gas sensors and biosensors. The ZnO semiconductor in the form of porous layer as well as in the form of nanostructures (nanotubes and nanoparticles) is used as a sensor layer for detection of the following gaseous environment: NH_3, NO_2, H_2 (Struk et al., 2015; Procek et al., 2016). The porous and nanostructures ZnO layers are also applied in biosensors for detection of protein G, DNA, dopamine, glucose, proteins (BSA HSA), rabbit IgG, cancer cells, and cholesterol (Tereshchenko et al., 2016). From the view point of application of ZnO semiconductor in biomedical engineering and biosensors, it should be mentioned that the ZnO is also biocompatible material (Gopikrishnan et al., 2010).

14.4 Conclusions

In this chapter, we have presented an overview of fiber-optic sensors with nanolayers and thin films for biosensing applications. We focused on the use of carbon-based nanolayers (e.g., NCD, B-NCD) as well as noncarbon-based nanolayers (ZnO), TiO2, which have been successfully applied in the construction of such sensors. The presented sensors have been used for the optical characterization of biological tissue such as: blood, cells, etc. The sensors enable measurements without the need for additional preparation of samples. Furthermore, the amount of biological tissue needed for measurement is negligible (less than a single microliter) and the measurement time does not exceed seconds.

Due to potential miniaturization and simple handling, the fiber-optic biosensors offer unique capabilities for noninvasive or minimally invasive clinical applications. The immunity to electromagnetic interference and the absence of electrical contact make these sensors useful for keeping only the sensitive element near the patient's bed and installing the optoelectronics in a safer location. In fact, there are many optical fiber sensors designed for biomedical applications and described in the literature, but most of them need clinical validation to fulfill the requirements of the European Directives on Medical Devices or the regulations of the Food and Drug Administration before entering the hospital.

Acknowledgments

References

Amaral, M., Dias, A.G., Gomes, P.S., Lopes, M.A., Silva, R.F., Santos, J.D., et al., 2008. Nanocrystalline diamond: In vitro biocompatibility assessment by MG63 and human bone marrow cells cultures. J. Biomed. Mater. Res. A 87A, 91−99.

Avino, S., D'Avino, V., Giorgini, A., Pacelli, R., Liuzzi, R., Cella, L., et al., 2013. Detecting ionizing radiation with optical fibers down to biomedical doses. Appl. Phys. Lett. 103, 184102.

Bajaj, P., Akin, D., Gupta, A., Sherman, D., Shi, B., Auciello, O., et al., 2007. Ultrananocrystalline diamond film as an optimal cell interface for biomedical applications. Biomed. Microdevices 9, 787−794.

Baldini, F., Giannetti, A., Mencaglia, A.A., Trono, C., 2008. Fiber optic sensors for biomedical applications. Current Analyt. Chem. 4 (4), 378−390.

Bilitewski, U., Bier, F., Brandenburg, A., 1998. Immunobiosensors based on grating couplers. Affinity Biosensors, Methods in Biotechnology. Humana Press, pp. 121−134.

Binghui, L., Heongkyu, J., 2013. Label-free optical biosensors based on a planar optical waveguide. BioChip J. 7, 295−318.

Bogdanowicz, R., 2014. Characterization of optical and electrical properties of transparent conductive boron-doped diamond thin films grown on fused silica. Metrol. Meas. Syst. 21, 685−698.

Bogdanowicz, R., Czupryniak, J., Gnyba, M., Ryl, J., Ossowski, T., Sobaszek, M., et al., 2013. Amperometric sensing of chemical oxygen demand at glassy carbon and silicon electrodes modified with boron-doped diamond. Sens. Actuators B Chem. 189, 30−36.

Bogdanowicz, R., Smietana, M., Gnyba, M., Golunski, L., Ryl, J., Gardas, M., 2014. Optical and structural properties of polycrystalline CVD diamond films grown on fused silica optical fibres pre-treated by high-power sonication seeding. Appl. Phys. -Mater. Sci. Process. 116, 1927−1937.

Bohnert, K., Gabus, P., Kostovic, J., Brändle, H., 2005. Optical fiber sensors for the electric power industry. Opt. Lasers Eng. 43, 511−526. Optics in Switzerland.

Bosch, M.E., Sánchez, A.J.R., Rojas, F.S., Ojeda, C.B., 2007. Recent Development in Optical Fiber Biosensors. Sensors 7, 797−859.

Brillas, E., Martínez-Huitle, C.A., 2011. Synthetic diamond films preparation. electrochemistry, characterization, and applications. John Wiley & Sons, Inc, Hoboken, N.J.

Brynda, E., Houska, M., Brandenburg, A., Wikerstal, A., Skvor, J., 1999. The detection of human beta 2-microglobulin by grating coupler immunosensor with three dimensional antibody networks. Biosens. Bioelectron. 14, 363−368.

Cabello-Aguilar, S., Balme, S., Chaaya, A.A., Bechelany, M., Balanzat, E., Janot, J.-M., et al., 2013. Slow translocation of polynucleotides and their discrimination by α-hemolysin inside a single track-etched nanopore designed by atomic layer deposition. Nanoscale 5, 9582−9586.

Checoury, X., Néel, D., Boucaud, P., Gesset, C., Girard, H., Saada, S., et al., 2012. Nanocrystalline diamond photonics platform with high quality factor photonic crystal cavities. Appl. Phys. Lett. 101, 171115.

Chiavaioli, F., Gouveia, C., Jorge, P., Baldini, F., 2017. Towards a uniform metrological assessment of grating-based optical fiber sensors: from refractometers to biosensors. Biosensors 7, 23.

Chiavaioli, F., Biswas, P., Trono, C., Jana, S., Bandyopadhyay, S., Basumallick, N., et al., 2015. Sol−Gel-based titania−silica thin film overlay for long period fiber grating-based biosensors. Anal. Chem. 87, 12024−12031.

Choi, J.Y., Lee, Y.-J., Shin, J., Yang, J.-W., 2010. Anodic oxidation of 1,4-dioxane on boron-doped diamond electrodes for wastewater treatment. J. Hazard. Mater. 179, 762−768.

Clerc, D., Lukosz, W., 1997. Direct immunosensing with an integrated-optical output grating coupler. Sens. Actuators B Chem. 40, 53−58.

Coelho, L., Viegas, D., Santos, J.L., de Almeida, J.M.M.M., 2014. Enhanced refractive index sensing characteristics of optical fibre long period grating coated with titanium dioxide thin films. Sens. Actuators B Chem. 202, 929−934.

Coelho, L., de Almeida, J.M.M.M., Santos, J.L., Ferreira, R.A.S., André, P.S., Viegas, D., 2015. Sensing structure based on surface plasmon resonance in chemically etched single mode optical fibres. Plasmonics 10, 319−327.

Coelho, L., Marques Martins de Almeida, J.M., Santos, J.L., da Silva Jorge, P.A., Martins, M.C.L., Viegas, D., et al., 2016. Aptamer-based fiber sensor for thrombin detection. J. Biomed. Opt. 21, 87005.

Davanlou, A., 2014. Integration of fiber-optic sensors in measuring machines. Measurement 57, 25−32.

Dominik, M., Leśniewski, A., Janczuk, M., Niedziółka-Jönsson, J., Hołdyński, M., Wachnicki, Ł., et al., 2017. Titanium oxide thin films obtained with physical and chemical vapour deposition methods for optical biosensing purposes. Biosens. Bioelectron. 93, 102−109.

Drobek, M., Bechelany, M., Vallicari, C., Abou Chaaya, A., Charmette, C., Salvador-Levehang, C., et al., 2015. An innovative approach for the preparation of confined ZIF-8 membranes by conversion of ZnO ALD layers. J. Membr. Sci. 475, 39−46.

Drobek, M., Kim, J.-H., Bechelany, M., Vallicari, C., Julbe, A., Kim, S.S., 2016. MOF-based membrane encapsulated ZnO nanowires for enhanced gas sensor selectivity. ACS Appl. Mater. Interfaces 8, 8323−8328.

Fabisiak, K., Szreiber, M., Uniszkiewicz, C., Runka, T., Kasprowicz, D., 2010. Electron paramagnetic resonance and raman spectroscopy characterization of diamond films fabricated by HF CVD method. Cryst. Res. Technol. 45, 167−172.

Fierro, S., Seishima, R., Nagano, O., Saya, H., Einaga, Y., 2013. In vivo pH monitoring using boron doped diamond microelectrode and silver needles: application to stomach disorder diagnosis. Sci. Rep. 3, srep03257.

Gajewski, W., Achatz, P., Williams, O.A., Haenen, K., Bustarret, E., Stutzmann, M., et al., 2009. Electronic and optical properties of boron-doped nanocrystalline diamond films. Phys. Rev. B 79, 45206.

Gao, D., Guan, C., Wen, Y., Zhong, X., Yuan, L., 2014. Multi-hole fiber based surface plasmon resonance sensor operated at near-infrared wavelengths. Opt. Commun. 313, 94−98.

Gartmann, T.E., Kehl, F., 2015. Experimental validation of the sensitivity of waveguide grating based refractometric (bio)sensors. Biosensors 5, 187−198.

Gopikrishnan, R., Zhang, K., Ravichandran, P., Baluchamy, S., Ramesh, V., Biradar, S., et al., 2010. Synthesis, characterization and biocompatibility studies of zinc oxide (ZnO) nanorods for biomedical application. Nano-Micro Letters 2, 31−36.

Grattan, K.T.V., 2000. Optical Fiber Sensor Technology. Kluwer Academic Publisher, Boston, MA, USA.

Hariharan, P., 2003. Optical Interferometry. Academic Press, San Diego.

Heideman, R.G., Lambeck, P.V., Gardeniers, J.G.E., 1995. High quality ZnO layers with adjustable refractive indices for integrated optics applications. Opt. Mater. 4, 741−755.

Hirsch, M., Wierzba, P., Jędrzejewska-Szczerska, M., 2016. Application of thin dielectric films in low coherence fiber-optic Fabry-Pérot sensing interferometers: comparative study, 101610D.

Hirsch, M., Majchrowicz, D., Wierzba, P., Weber, M., Bechelany, M., Jędrzejewska-Szczerska, M., 2017. Low-coherence interferometric fiber-optic sensors with potential applications as biosensors. Sensors 17, 261.

Hu, Z.G., Hess, P., 2006. Optical constants and thermo-optic coefficients of nanocrystalline diamond films at 30−500 °C. Appl. Phys. Lett. 89, 81906-81906−3.

Hu, Z.G., Prunici, P., Hess, P., Chen, K.H., 2007. Optical properties of nanocrystalline diamond films from mid-infrared to ultraviolet using reflectometry and ellipsometry. J. Mater. Sci. Mater. Electron. 18, 37−41.

Hunsperger, R.G., 2009. Integrated Optics Theory and Technology. Springer, Berlin.

Iniesta, J., Michaud, P.A., Panizza, M., Cerisola, G., Aldaz, A., Comninellis, C., 2001. Electrochemical oxidation of phenol at boron-doped diamond electrode. Electrochimica Acta 46, 3573−3578.

Jagadish, C., Pearton, S., 2006. Zinc Oxide Bulk - Thin Films and Nanostructures. Elsevier.

Janczuk-Richter, M., Dominik, M., Roźniecka, E., Koba, M., Mikulic, P., Bock, W.J., et al., 2017. Long-period fiber grating sensor for detection of viruses. Sens. Actuators B Chem. 250, 32−38.

Jędrzejewska-Szczerska, M., Wierzba, P., Chaaya, A.A., Bechelany, M., Miele, P., Viter, R., et al., 2015. ALD thin ZnO layer as an active medium in a fiber-optic Fabry−Perot interferometer. Sens. Actuators Phys. 221, 88−94.

Kalish, R., 1999. Doping of diamond. Carbon 37, 781−785.

Klantsataya, E., Jia, P., Ebendorff-Heidepriem, H., Monro, T., François, A., 2016. Plasmonic fiber optic refractometric sensors: from conventional architectures to recent design trends. Sensors 17, 12.

Kromka, A., Rezek, B., Remes, Z., Michalka, M., Ledinsky, M., Zemek, J., et al., 2008. Formation of continuous nanocrystalline diamond layers on glass and silicon at low temperatures. Chem. Vap. Depos. 14, 181−186.

Lambeck, P.V., 2006. Integrated optical sensors for the chemical domain. Meas. Sci. Technol. 17, R93.

Le, T.X.H., Esmilaire, R., Drobek, M., Bechelany, M., Vallicari, C., Nguyen, D.L., et al., 2016. Design of a novel fuel cell-Fenton system: a smart approach to zero energy depollution. J. Mater. Chem. A 4, 17686−17693.

Le, T.X.H., Esmilaire, R., Drobek, M., Bechelany, M., Vallicari, C., Cerneaux, S., et al., 2017. Nitrogen-doped graphitized carbon electrodes for biorefractory pollutant removal. J. Phys. Chem. C 121, 15188−15197.

Long, F., Zhu, A., Shi, H., 2013. Recent advances in optical biosensors for environmental monitoring and early warning. Sensors 13, 13928−13948.

Lukosz, W., 1995. Integrated optical chemical and direct biochemical sensors. Sens. Actuators B Chem. 37−50.

Lukosz, W., Tiefenthaler, K., 1988. Sensitivity of integrated optical grating and prism couplers as (bio)chemical sensors. Sens. Actuators 15, 273−284.

Maguire, P.D., McLaughlin, J.A., Okpalugo, T.I.T., Lemoine, P., Papakonstantinou, P., McAdams, E.T., et al., 2005. Mechanical stability, corrosion performance and bioresponse of amorphous diamond-like carbon for medical stents and guidewires. Diam. Relat. Mater. 14, 1277−1288.

Majchrowicz, D., Den, W., Hirsch, M., 2016a. The low coherence Fabry-Pérot interferometer with diamond and ZnO layers. Proc. SPIE. 10031, 1003112−1003112−6.

Majchrowicz, D., Den, W., Jędrzejewska-Szczerska, M., 2016b. Application of boron-doped diamond film and ZnO layer in the Fabry-Pérot interferometer. Proc. SPIE 10034, 1003408−1003408−6.

Majchrowicz, D., Hirsch, M., Wierzba, P., Bechelany, M., Viter, R., Jędrzejewska-Szczerska, M., 2016c. Application of thin ZnO ALD layers in fiber-optic Fabry-Pérot sensing interferometers. Sensors 16, 416.

Marichy, C., Bechelany, M., Pinna, N., 2012. Atomic layer deposition of nanostructured materials for energy and environmental applications. Adv. Mater. 24, 1017−1032.

McCreery, R.L., 2008. Advanced carbon electrode materials for molecular electrochemistry. Chem. Rev. 108, 2646−2687.

Mermoux, M., Marcus, B., Swain, G.M., Butler, J.E., 2002. A confocal Raman imaging study of an optically transparent boron-doped diamond electrode. J. Phys. Chem. B 106, 10816−10827.

Milewska, D., Karpienko, K., Jędrzejewska-Szczerska, M., 2016. Application of thin diamond films in low-coherence fiber-optic Fabry Pérot displacement sensor. Diam. Relat. Mater. 64, 169−176.

Mohl, M., Dombovari, A., Rautio, A.-R., Tuchina, E.S., Petrov, P.O., Bibikova, O.A., et al., 2014. Gypsum-titania fiber nanocomposites for indoor antimicrobial coatings. Journal of Materials Chemistry B. 2, 1307−1316.

Montanaro, D., Lavecchia, R., Petrucci, E., Zuorro, A., 2017. UV-assisted electrochemical degradation of coumarin on boron-doped diamond electrodes. Chem. Eng. J. 323, 512−519.

Mukundan, H., Anderson, A.S., Grace, W.K., Grace, K.M., Hartman, N., Martinez, J.S., et al., 2009. Waveguide-based biosensors for pathogen detection. Sensors 9, 5783−5809.

Nebel, C.E., Rezek, B., Shin, D., Uetsuka, H., Yang, N., 2007. Diamond for bio-sensor applications. J. Phys. Appl. Phys. 40, 6443.

Niedziałkowski, P., Bogdanowicz, R., Zięba, P., Wysocka, J., Ryl, J., Sobaszek, M., et al., 2016. Melamine-modified boron-doped diamond towards enhanced detection of adenine, guanine and caffeine. Electroanalysis 28, 211−221.

Opilski, A., 2002. Laboratorium optoelektroniki światłowodowej. Wydawnictwo Politechniki Śląskiej.

Özgür, Ü., Alivov, Y.I., Liu, C., Teke, A., Reshchikov, M.A., Doğan, S., et al., 2005. A comprehensive review of ZnO materials and devices. J. Appl. Phys. 98, 41301.

Pathak, A.K., Bhardwaj, V., Gangwar, R.K., De, M., Singh, V.K., 2017. Fabrication and characterization of TiO2 coated cone shaped nano-fiber pH sensor. Opt. Commun. 386, 43−48.

Piehler, J., Brandenburg, A., Brecht, A., Wagner, E., Gauglitz, G., 1997. Characterization of grating couplers for affinity-based pesticide sensing. Appl. Opt. 36, 6554−6562.

Pluciński, J., Karpienko, K., 2016. Fiber optic Fabry-Pérot sensors: modeling versus measurements results. Proc. SPIE 10034, 100340H−100340H−7.

Pospíšilová, M., Kuncová, G., Trögl, J., 2015. Fiber-optic chemical sensors and fiber-optic bio-sensors. Sensors 15, 25208−25259.

Potocky, S., Kromka, A., Potmesil, J., Remes, Z., Vorlicek, V., Vanecek, M., et al., 2007. Investigation of nanocrystalline diamond films grown on silicon and glass at substrate temperature below 400 °C. Diam. Relat. Mater. 744−747.

Procek, M., Pustelny, T., Stolarczyk, A., 2016. Influence of external gaseous environments on the electrical properties of zno nanostructures obtained by a hydrothermal method. Nanomaterials 6, 1−17.

Pustelny, T., Struk, P., 2012. Numerical analyses of optical couplers for planar waveguides. Opto-Electron. Rev. 20, 201−206.

Puyol, M., Villuendas, F., Domínguez, C., Cadarso, V., Llobera, A., Salinas, I., et al., 2005. Absorbance-based integrated optical sensors. Frontiers in Chemical Sensors, Springer Series on Chemical Sensors and Biosensors. Springer, Berlin, Heidelberg, pp. 1−44.

Remes, Z., 2010. High optical quality nanocrystalline diamond with reduced non-diamond contamination. Diam. Relat. Mater. 453−456.

Rifat, A.A., Mahdiraji, G.A., Sua, Y.M., Ahmed, R., Shee, Y.G., Adikan, F.R.M., 2016. Highly sensitive multi-core flat fiber surface plasmon resonance refractive index sensor. Opt. Express 24, 2485.

Rozycki-Bakon, R., Koba, M., Firek, P., Rozniecka, E., Niedziolka-Jonsson, J., Smietana, M., 2016. Stack of nano-films on optical fiber end face for label-free bio-recognition. J. Light. Technol. 34, 5357−5362.

Sarkar, A., Shchukarev, A., Leino, A.-R., Kordas, K., Mikkola, J.-P., Petrov, P.O., et al., 2012. Photocatalytic activity of TiO2 nanoparticles: effect of thermal annealing under various gaseous atmospheres. Nanotechnology 23, 475711-1-8.

Shabaneh, A., Girei, S., Arasu, P., Mahdi, M., Rashid, S., Paiman, S., et al., 2015. Dynamic response of tapered optical multimode fiber coated with carbon nanotubes for ethanol sensing application. Sensors 15, 10452−10464.

Shiomi, H., Nishibayashi, Y., Fujimori, N., 1991. Characterization of boron-doped diamond epitaxial films. Jpn. J. Appl. Phys. 30, 1363−1366.

Singh, S., Mishra, S.K., Gupta, B.D., 2013. Sensitivity enhancement of a surface plasmon resonance based fibre optic refractive index sensor utilizing an additional layer of oxides. Sens. Actuators Phys. 193, 136−140.

Skibina, Y.S., Tuchin, V.V., Beloglazov, V.I., Shteinmaeer, G., Betge, I.L., Wedell, R., et al., 2011. Photonic crystal fibres in biomedical investigations. Quantum Electron. 41, 284−301.

Smietana, M., Szmidt, J., Korwin-Pawlowski, M.L., Bock, W.J., Grabarczyk, J., 2007. Application of diamond-like carbon films in optical fibre sensors based on long-period gratings. Diam. Relat. Mater. 1374−1377.

Smietana, M., Koba, M., Brzozowska, E., Krogulski, K., Nakonieczny, J., Wachnicki, L., et al., 2015. Label-free sensitivity of long-period gratings enhanced by atomic layer deposited TiO_2 nano-overlays. Opt. Express 23, 8441.

Sobaszek, M., Siuzdak, K., Skowroński, Ł., Bogdanowicz, R., Pluciński, J., 2016. Optically transparent boron-doped nanocrystalline diamond films for spectroelectrochemical measurements on different substrates. IOP Conf. Ser. Mater. Sci. Eng. 104, 12024.

Spitsyn, B.V., Bouilov, L.L., Derjaguin, B.V., 1981. Vapor growth of diamond on diamond and other surfaces. J. Cryst. Growth 52 (Part 1), 219−226.

Stavis, C., Clare, T.L., Butler, J.E., Radadia, A.D., Carr, R., Zeng, H., et al., 2011. Surface functionalization of thin-film diamond for highly stable and selective biological interfaces. Proc. Natl. Acad. Sci. 108, 983−988.

Stotter, J., Zak, J., Behler, Z., Show, Y., Swain, G.M., 2002. Optical and electrochemical properties of optically transparent, boron-doped diamond thin films deposited on quartz. Anal. Chem. 74, 5924−5930.

Stotter, J., Haymond, S., Zak, J.K., Show, Y., Cvackova, Z., Swain, G.M., 2003. Optically transparent diamond electrodes for UV-Vis and IR spectroelectrochemistry. Interface 12, 33−38.

Struk, P., Pustelny, T., Gut, K., Gołaszewska, K., Kamińska, E., Ekielski, M., et al., 2009. Planar optical waveguides based on thin ZnO Layers. Acta Phys. Pol. A 116, 414−418.

Struk, P., Pustelny, T., Gołaszewska, K., Kamińska, E., Borysiewicz, M., Ekielski, M., et al., 2011. Photonic structures with grating couplers based on ZnO. Opto-Electron. Rev. 19, 462.

Struk, P., Pustelny, T., Gołaszewska, K., Kamińska, E., Borysiewicz, M.A., Ekielski, M., et al., 2013. Hybrid photonics structures with grating and prism couplers based on ZnO waveguides. Opto-Electron. Rev. 21, 376−381.

Struk, P., Pustelny, T., Gołaszewska, K., Borysiewicz, M.A., Kamińska, E., Wojciechowski, T., et al., 2014. Wide bandgap semiconductor and possibilities of its application in optical waveguide structures. Metrol. Meas. Syst. 21, 401−412.

Struk, P., Pustelny, T., Gołaszewska, K., Borysiewicz, M.A., Piotrowska, A., 2015. Optical investigations of ZnO layers affected by some selected gases in the aspect of their application in optical gas sensors. Bull. Pol. Ac.: Tech. 63, 829−836.

Sukhadolau, A.V., Ivakin, E.V., Ralchenko, V.G., Khomich, A.V., Vlasov, A.V., Popovich, A.F., 2005. Thermal conductivity of CVD diamond at elevated temperatures. Diam. Relat. Mater. 14, 589−593.

Swain, G.M., Anderson, A.B., Angus, J.C., 1998. Applications of diamond thin films in electrochemistry. MRS Bull. 23, 56−60.

Tereshchenko, A., Bechelany, M., Viter, R., Khranovskyy, V., Smyntyna, V., Starodub, N., et al., 2016. Optical biosensors based on ZnO nanostructures: advantages and perspectives. A review. Sens. Actuators B Chem. 229, 664−677.

Tiefenthaler, K., Lukosz, W., 1989. Sensitivity of grating couplers as integrated-optical chemical sensors. JOSA B 6, 209−220.

Tubchareon, T., Soisuwan, S., Ratanathammaphan, S., Praserthdam, P., 2013. Effect of Na-, K-, Mg-, and Ga dopants in A/B-sites on the optical band gap and photoluminescence behavior of TiO3 powders. J. Lumin. 142, 75−80.

Vörös, J., Ramsden, J.J., Csúcs, G., Szendrő, I., De Paul, S.M., Textor, M., et al., 2002. Optical grating coupler biosensors. Biomaterials 23, 3699−3710.

Waldhäusl, R., Schnabel, B., Dannberg, P., Kley, E.B., Bräuer, A., Karthe, W., 1997. Efficient coupling into polymer waveguides by gratings. Appl. Opt. 36, 9383−9390.

Wang, X., Wolfbeis, O.S., 2016. Fiber-optic chemical sensors and biosensors. Anal. Chem. 88, 203−227.

Wang, Y.-M., Pang, X.-F., Zhang, Y.-Y., 2009. Recent advances in fiber-optic DNA biosensors. J. Biomed. Sci. Eng. 2, 312.

Williams, O.A., Nesládek, M., 2006. Growth and properties of nanocrystalline diamond films. Phys. Status Solidi A 203, 3375−3386.

Wu, H., Xiao, S., Chen, D., Qasim, A.M., Ding, K., Wu, G., et al., 2017. Effects of diamond-like carbon film on the corrosion behavior of NdFeB permanent magnet. Surf. Coat. Technol. 312, 66−74. 13th International Conference on Plasma-Based Ion Implantation and Deposition.

Wurzinger, P., Pongratz, P., Hartmann, P., Haubner, R., Lux, B., 1997. Investigation of the boron incorporation in polycrystalline CVD diamond films by TEM, EELS and Raman spectroscopy. Diam. Relat. Mater. 6, 763−768.

Yang, R.-Z., Dong, W.-F., Meng, X., Zhang, X.-L., Sun, Y.-L., Hao, Y.-W., et al., 2012. Nanoporous TiO$_2$/polyion thin-film-coated long-period grating sensors for the direct measurement of low-molecular-weight analytes. Langmuir 28, 8814−8821.

Yariv, A., Nakamura, M., 1977. Periodic structures for integrated optics. IEEE J. Quantum Electron. 13, 233−253.

Yeap, W.S., Bevk, D., Liu, X., Krysova, H., Pasquarelli, A., Vanderzande, D., et al., 2014. Diamond functionalization with light-harvesting molecular wires: improved surface coverage by optimized Suzuki cross-coupling conditions. RSC Adv. 4, 42044−42053.

Zanishevskaya, A.A., Shuvalov, A.A., Skibina, Y.S., Tuchin, V.V., 2015. Blood typing using microstructured waveguide smart cuvette. J. Biomed. Opt. 20 (4), 040503.

Zhao, W., Xu, J.-J., Qiu, Q.-Q., Chen, H.-Y., 2006. Nanocrystalline diamond modified gold electrode for glucose biosensing. Biosens. Bioelectron. 22, 649−655.

Zheng, W., van den Hurk, R., Cao, Y., Du, R., Sun, X., Wang, Y., et al., 2016. Aryl diazonium chemistry for the surface functionalization of glassy biosensors. Biosensors 6.

Zhou, Y., Zhi, J., 2009. The application of boron-doped diamond electrodes in amperometric biosensors. Talanta 79, 1189−1196.

Zhu, J.-T., Shi, C.-G., Xu, J.-J., Chen, H.-Y., 2007. Direct electrochemistry and electrocatalysis of hemoglobin on undoped nanocrystalline diamond modified glassy carbon electrode. Bioelectrochemistry 71, 243−248.

Zhu, S., Pang, F., Huang, S., Zou, F., Guo, Q., Wen, J., et al., 2016. High sensitivity refractometer based on TiO2-coated adiabatic tapered optical fiber via ALD technology. Sensors 16, 1295.

Zuerbig, V., Pletschen, W., Hees, J., Sah, R.E., Kirste, L., Heidrich, N., et al., 2013. Transparent diamond electrodes for tunable micro-optical devices. Diam. Relat. Mater. 38, 101−103.